Modulated-photocurrent spectroscopy of highly crystalline organic

semiconducting materials with pristine and trap-dominated surfaces.

P. Kounavis¹ and V. Podzorov²

¹Department of Electrical and Computer Engineering, University of Patras, 26504, Patra,

Greece

²Department of Physics, Rutgers University, Piscataway, NJ 08854, USA

ABSTRACT

High-mobility organic semiconductors are investigated by a novel modulated

photocurrent spectroscopy for the first time. In this technique, modulated and steady-state

photocarrier populations are independently generated and controlled by two light beams in a

benchmark organic semiconductor *rubrene*. The technique allowed identifying a band-like

carrier motion (as opposed to hopping) as the dominant charge transport mechanism in this

highly crystalline molecular semiconductor, in agreement with prior studies, yet without the

need for fabrication of complex transistor devices. Our study also yields the distribution and

density of trap states that can be as low as $\sim 10^{13}$ cm⁻³·eV⁻¹ in pristine crystals. Additionally,

we demonstrate that the ubiquitous, yet mysterious effect of semiconducting materials'

degradation in high vacuum environments, known as the "gauge effect", corresponds to a

drastic increase of hole trap density at the surface of the semiconductor (by at least on order

of magnitude), when the material is exposed to an operating high-vacuum pressure gauge,

leading to a strong decrease of the surface carrier mobility. This work demonstrates the

power of the modulated photocurrent spectroscopy in unraveling the relevant electronic

properties of high-performance organic semiconductors and, more broadly, other advanced

electronic materials.

Corresponding author. E-mail address: pkounavis@upatras.gr (P. Kounavis).

1

I. INTRODUCTION

High-purity single crystals of a small-molecule organic semiconductor *rubrene* ($C_{42}H_{28}$) exhibit comparatively high photoconductivity (PC) in the visible spectral range, for wavelengths $400 < \lambda < 560$ nm, where rubrene is an efficient light absorber. A variety of optoelectronic devices based on crystalline organic semiconductors, including photodetectors and solar cells, are envisioned [1-9]. It would thus be very important to understand the fundamental processes of photocarrier generation, transport and charge interactions with traps in benchmark organic semiconductors, such as rubrene. The modulated photocurrent (MPC) spectroscopy is a technique that has been proven powerful for investigating interactions of the majority carriers with traps in inorganic semiconductors [10]. More recently, MPC spectroscopy has been also applied to polycrystalline thin-films of pentacene ($C_{22}H_{14}$), in which it allowed determining the dominant charge transport mechanism, extracting the distribution of trap states and evaluate the impact of steady-state illumination on charge carrier mobility [11].

Here MPC measurements are carried out in a crystalline high-performance organic semiconductor (rubrene) for the first time. In this technique, a sample is illuminated with a monochromatic beam of light periodically modulated at a frequency ω (the so-called "probe" beam), while an ac photocurrent generated by this beam is detected by a lock-in amplifier tuned to the same frequency. This phase sensitive detection technique allows significantly improving the signal-to-noise ratio in measurements of photoconductivity. Simultaneously, the sample is subjected to an additional continuous-wave (cw) photoexcitation with a secondary light beam (called a "bias" beam). The additional excitation can affect the properties of photocarriers generated by the probe. The relative phase and amplitude of thus obtained ac-photoconductivity, recorded under a cw bias beam of varied intensity, carry the information about the mobility of photocarriers, their transport mechanism, and the density of

states (DOS) of localized states (traps) in the semiconductor's band gap. For instance, we demonstrate that a very interesting degradation effect of organic semiconductors, called a "gauge effect", can be efficiently studied by the MPC technique. The gauge effect refers to a drastic deterioration of the charge transport characteristics of organic semiconductors' surfaces induced by exposure of samples to operating high-vacuum pressure gauges [12]. We reveal in detail the pronounced changes induced by an ion gauge in the DOS of traps in rubrene single crystals, their distribution in the band gap, as well as the effect of these traps on the charge carrier mobility.

II. EXPERIMENTAL SECTION

A. Sample preparation.

Rubrene single crystals with typical dimensions of (a,b)-facets in the range 1 - 3 mm and thickness 0.1 - 1 mm were grown by a physical vapor transport following the previously published procudure [13]. Selected single crystals with well-defined facets were attached to substrates using tiny dropletts of rubber cement glue, and the source and drain contacts were painted with an aqueous suspension of colloidal graphite (carbon paint) that upon drying provides a good electrical contact to rubrene. Device wiring was done using a 25 μ m-thick gold wire.

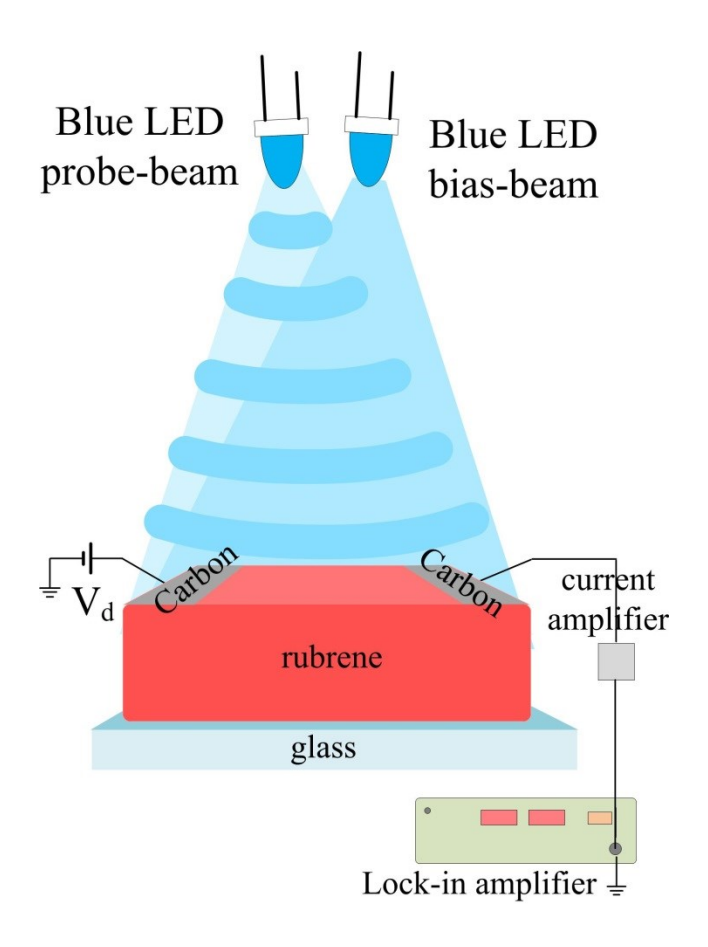


Figure 1. The modulated photocurrent (MPC) spectroscopy technique. Two blue LEDs ($\lambda = 460$ nm) are used to photoexcite a rubrene single crystal connected to an electric circuitry. The output of one of the LEDs is sinusoidally modulated at a frequency ω (the probe beam). The other LED provides a steady-state cw photoexcitation (the bias beam). The resultant photoconductivity of rubrene is measured by a lock-in amplifier tuned to the modulation frequency ω of the probe beam. The frequency ω of the probe beam, as well as the intensity of the bias beam can be varied.

B. Photo-current excitation spectroscopy.

Photocurrent excitation (PCE) spectroscopy was carried out under a cw illumination. The source of illumination was a monochromatic output from a Cornerstone-Oriel monochromator passed through a filter and focused on the crystal. During the PCE measurements, the crystal was kept in an optical cryostat at $\sim 10^{-1}$ Torr. The intensity (or

power density), F, of incident light was tuned by using neutral density filters and measured with a calibrated photodetector. A small dc source-drain voltage, $V_{\rm SD} \approx 1$ - 5 V, was applied between the graphite source and drain contacts with a Keithley 2400 source-meter, and the resulting photocurrent, $I_{\rm SD}$, flowing through the crystal was measured with Keithley 617 or 6517B electrometers.

C. Modulated photocurrent (MPC) spectroscopy.

In MPC measurements, the input voltage of a blue LED (λ = 460 nm) is sinusoidally modulated and the resulting modulated light emitted from the LED at a frequency in the range ω = 0.8 - 10⁵ Hz is used as the probe beam. The beam is incident at a free (a,b)-facet of a rubrene single crystal, as schematically shown in Fig. 1. A population of photocarriers with a density modulated at this frequency is generated in the crystal, producing an MPC signal that is amplified and measured by a lock-in amplifier (Stanford Research SR830). The MPC's amplitude, I_{ac} , and phase shift, θ , relative to the phase of the probe beam, are the two main quantities measured in the MPC experiment. An additional photoexcitation by another blue LED, generating a cw light of the same wavelength (the bias beam), is used to create an additional steady-state population of carriers. The intensity of the probe beam is typically greater than that of the bias beam by at least a factor of three. The intensity of the bias beam can be varied, so that the additional steady-state photocarrier population and thus the position of the quasi-Fermi level within the band gap are controlled. The changes in the quasi-Fermi level's position are studied in reference to the corresponding changes in MPC spectra of the crystal.

MPC measurements can provide a wealth of information about the interaction of majority carriers with traps and can help in elucidating the relevant transport mechanism and parameters. While varying the modulation frequency ω , one can observe distinct features in

the *ac*-photocurrent in the high and low frequency domains that can be used to extract the information about the photocarrier transport, including the effect of illumination on carrier mobility, as well as the energetic distribution of traps within the bandgap.

III. RESULTS AND DISCUSSIONS

A. Photoconductivity as a function of incident illumination intensity.

The observed dependence of steady-state photocurrent I_p on the intensity F of incident cw illumination has a form: $I_p \sim F^\alpha$, with the power exponent $\alpha = 1$ (linear dependence) at low illumination intensities, and $\alpha \approx 0.33$ and 0.28 observed at relatively high intensities.

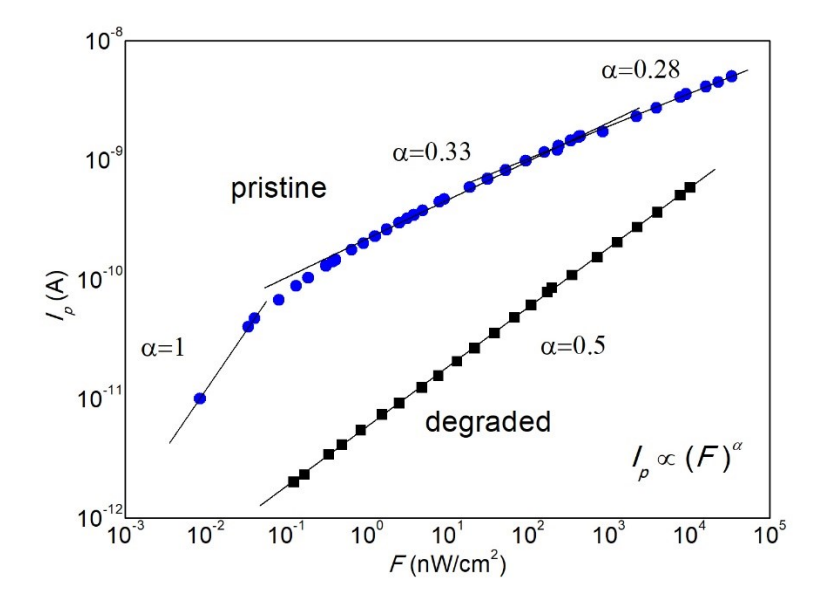


Figure 2. Photocurrent vs incident light intensity in a rubrene single crystal. Photoexcitation: a blue LED ($\lambda = 460$ nm). A pristine (blue circles) and a trap-dominated (black squares) states of the same crystal are shown. The trap-dominated ("degraded") state was prepared by exposing the pristine crystal to an operating high-vacuum ion gauge (for 5 s). The photocurrent exhibits a power-law dependence on the incident light intensity, $I_p \sim (F)^\alpha$, with the power exponent α sequentially taking the values 1, 1/3 and $\sim \frac{1}{4}$ in the pristine state, and $\alpha = \frac{1}{2}$ in the trap-dominated state.

When the crystal is briefly exposed to an operating ion gauge in high vacuum (by manually turning the gauge on and off when a sufficiently low pressure is reached), a very rapid decrease of the dark conductivity by a factor of ~ 10 is observed within the first few seconds of the gauge operation. The photoconductivity in thus prepared "degraded" state of the crystal is also found to be reduced by 1-1.5 orders of magnitude, with exponent $\alpha=0.5$ observed in the entire range of the studied illumination intensities. The observed power exponents and the gauge effect behavior are in agreement with the recent report by Irkhin *et al.* [14]. We use the gauge effect here to *intentionally* induce surface traps and study the corresponding changes in the crystal's photocarrier transport properties.

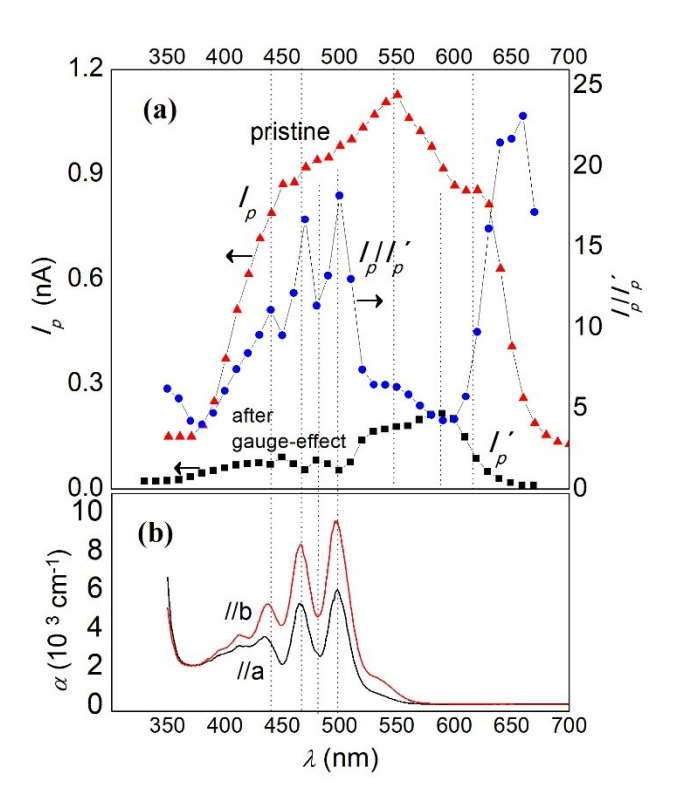


Figure 3. The photocurrent excitation spectra compared to the absorption spectra of rubrene.

(a) Photocurrent excitation spectra of a rubrene crystal in its pristine (red triangles) and trapdominated (black squares) states. The latter state was prepared by intentionally exposing the crystal to an operating high-vacuum gauge (the "gauge effect"). The ratio of the photocurrents in the pristine and trap-dominated states, I_p/I_p (blue circles), is also plotted. (b) The experimental absorption coefficient $\alpha(\lambda)$ of rubrene single crystals for light linearly polarized along the crystal's **b**-axis (red) and **a**-axis (black), normally incident on the (a,b)-facet of the crystal.

B. Spectral response of *cw* photoconductivity.

A spectral response of the photocurrent of a rubrene crystal at a constant excitation intensity of 1 μ W is shown at Fig. 3 for pristine, I_p , and degraded, I_p , states of the same crystal. In the pristine state, the photocurrent shows two broad maxima around 550 and 620 nm, while other bands corresponding to the vibronic structure of the absorption spectrum of the crystal cannot be discerned. The absence of these bands in the pristine state can be attributed to a long triplet exciton diffusion length leading to a "smeared" vibronic structure in the photo-current excitation spectra in rubrene [15]. It is remarkable the production of significant photocurrent above 520 nm, where optical absorption abruptly drops at very low levels. A possible interpretation of this behavior is as follows. In contrast to the high optical absorption around 500 nm where light is absorbed more in the crystal's surface within about 1μm, low optical absorption above 520 nm allows deeper light penetration within about 10 um and more uniform creation of triplet excitons via singlet fission through the crystal's volume. In this case, the average separation of the triplet excitons is relatively higher, providing a relatively lower probability of triplet-triplet annihilation. Moreover, triplet excitons created up to the deeper light penetration depths (within 10 µm), due to their high diffusion length over distances 2-8 µm [15], are able to diffuse up to the free surface where

may dissociate into mobile charge carriers, accounting for the important photocurrent above 520 nm.

Following exposure of the crystal to an ion-gauge, the photocurrent significantly decreases (Fig. 3), and two small bands with maxima around 450 and 475 nm emerge. The strongest degradation of the photocurrent is observed for wavelengths below 525. The measurement of the photocurrent of the degraded crystal produced above 600 nm needs longer waiting time, so that it can be deduced reliable conclusions concerning photocurrent degradation from these data. It is remarkable that the photoresponse ratio I_p/I_p (solid blue circles in Fig. 3) reveals sharp maxima occurring at the spectral positions exactly matching the maxima of the absorption spectrum $\alpha(\lambda)$ of rubrene (shown in panel (b)), with the overall spectral shape of this ratio in the region 350 - 600 nm closely resembling that of $\alpha(\lambda)$. Such a behavior is not coincidental: it is an indication that the degradation caused by the gauge is stronger at wavelengths of stronger optical absorption. Namely, the ion-gauge leads to a degradation of photoresponse predominately at the optical absorption maxima, where the strong light absorption takes place closer to the surface of the crystal. This observation is reasonable given the fact that exposure to an ion-gauge essentially affects the surface of the crystal, thus most strongly affecting the charge transport at or near the surface.

C. Modulated photocurrent (MPC) measurements.

1. The effect of bias illumination.

Figure 4 shows typical MPC phase shift $\theta(\omega)$ and amplitude $I_{ac}(\omega)$ spectra for a rubrene single crystal that initially had a pristine (high-purity) surface (panels (a) and (b)), but was then intentionally degraded by exposure to an operating high-vacuum ion gauge (panels (c) and (d)). The spectra were collected under a photoexcitation with a probe beam ($\lambda = 460 \text{ nm}$)

modulated at a frequency ω , with an additional cw bias photoexcitation of the same wavelength but varied intensity (different levels of bias illumination correspond to symbols of different colors). At high frequencies, the phase θ and amplitude I_{ac} are essentially independent of the bias illumination intensity. At low frequencies, a substantial decrease in both θ and I_{ac} is observed with an increasing intensity of bias illumination (indicated by the red arrows). Although these tendencies in MPC spectra are qualitatively similar to those recently observed in polycrystalline pentacene thin films [11], the results of the data analysis and conclusions drawn here for rubrene are qualitatively and quantitatively different.

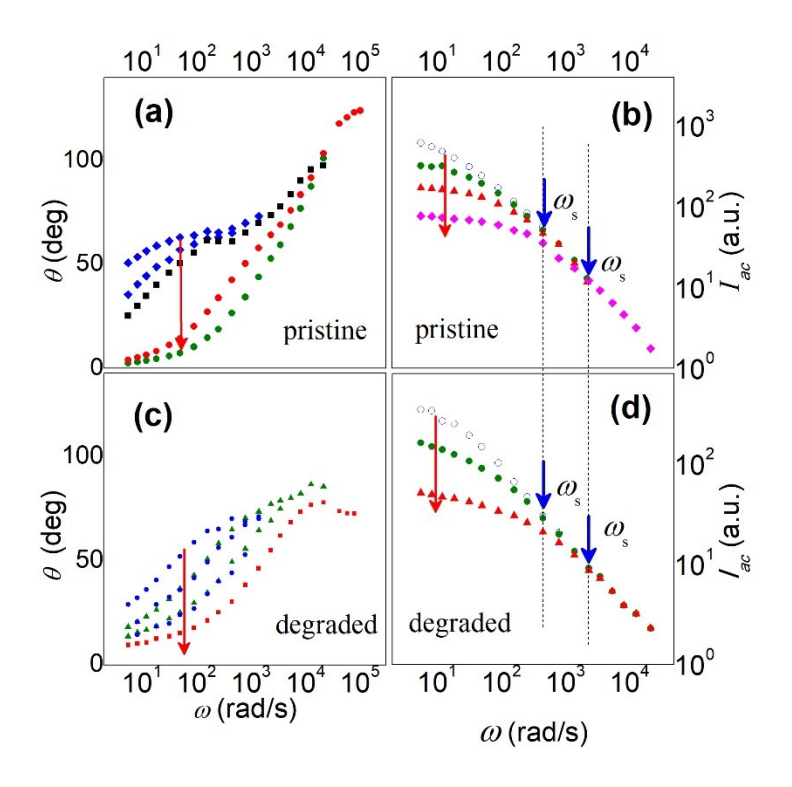


Figure 4. The MPC spectra of rubrene single crystals. The MPC phase shift θ and amplitude I_{ac} are shown in pristine and trap-dominated (degraded by an ion gauge) states of the same crystal.

Panels (a) and (b) correspond to the pristine state, while panels (c) and (d) correspond to the trapdominated state of the crystal. The data are plotted as a function of the modulation frequency ω of the probe beam. They are shown for various levels of additional cw bias illumination (corresponding to symbols of different color, with the red arrows pointing in the direction of increasing its intensity). Both the probe and the bias photoexcitations use the same type of a blue LED (λ = 460 nm). There are two regimes evident in these spectra: a low-frequency (LF) regime, in which a nearly zero phase shift and a plateau in the amplitude of MPC are reached, and the high-frequency (HF) regime, where the MPC phase shift is large, and the amplitude is strongly frequency-dependent.

Below we first briefly describe the principle of MPC spectral analysis, for which a more detailed theory is given in [10,11], and then analyze the data for rubrene shown in Fig. 4. Considering the general successes and applicability of the *multiple trap and release* (MTR) model of charge transport in organic semiconductors (see, e.g., [16], [17), one can think of the transport of photogenerated carriers as occurring via an ongoing competition between the carrier relaxation from extended (band) states to a distribution of localized in-gap (trap) states and thermal excitation of trapped carriers back into the band. The trap distribution in organic semiconductors usually takes a form of a tail of localized states, extending deep into the gap over considerable energies below the band edge (the so-called mobility edge). All energies are usually referred to with respect to this mobility edge. The tail includes both deep and shallow traps with energies, correspondingly, greater than and smaller than the thermal energy: $E_{\text{deep}} \ge kT$, and $0 < E_{\text{shallow}} \le kT$, where k is the Boltzmann constant, and T is absolute temperature. Considering here for simplicity only holes as majority carriers in rubrene and given the high density of states in the HOMO, one can think of charge transport as occurring entirely at a transport energy level matching the HOMO band edge (the mobility edge). It turns out that the contribution of hopping transport in localized tail states can be considered negligible, - we will show below that this conclusion is supported by our data. At

these conditions, the role of cw bias illumination is to excite carriers across the band gap of rubrene (2.2 eV), thus creating a population of mobile carriers that would quickly relax into the tail of localized states. They will partially fill the tail, starting from deepest levels (deep traps) and up to a certain characteristic energy level, $E_{\rm tp}$, that depends on the density of available photocarriers and trapping cross-section. The more photocarriers are generated, the more trap states in the tail are filled, and thus the closer $E_{\rm tp}$ level gets to the mobility edge. The role of the probe beam, on the other hand, is to selectively probe the contribution of a specific trap level with a characteristic energy $E_{\rm o}$ to photoconductivity. Since each trap within the tail is characterized by a certain carrier retention time (or, similarly, the carrier escape rate) that depends on the trap energy, the phase-sensitive detection of ac-photoconductivity with a probe beam modulated at a frequency ω predominantly probes the contribution of carriers trapped at and thermally released from the trap of the corresponding energy E_{ω} . In the MPC measurements, the relative energetic positions of thus defined energy levels, $E_{\rm tp}$ and E_{ω} , govern the phase shift and amplitude of MPC spectra.

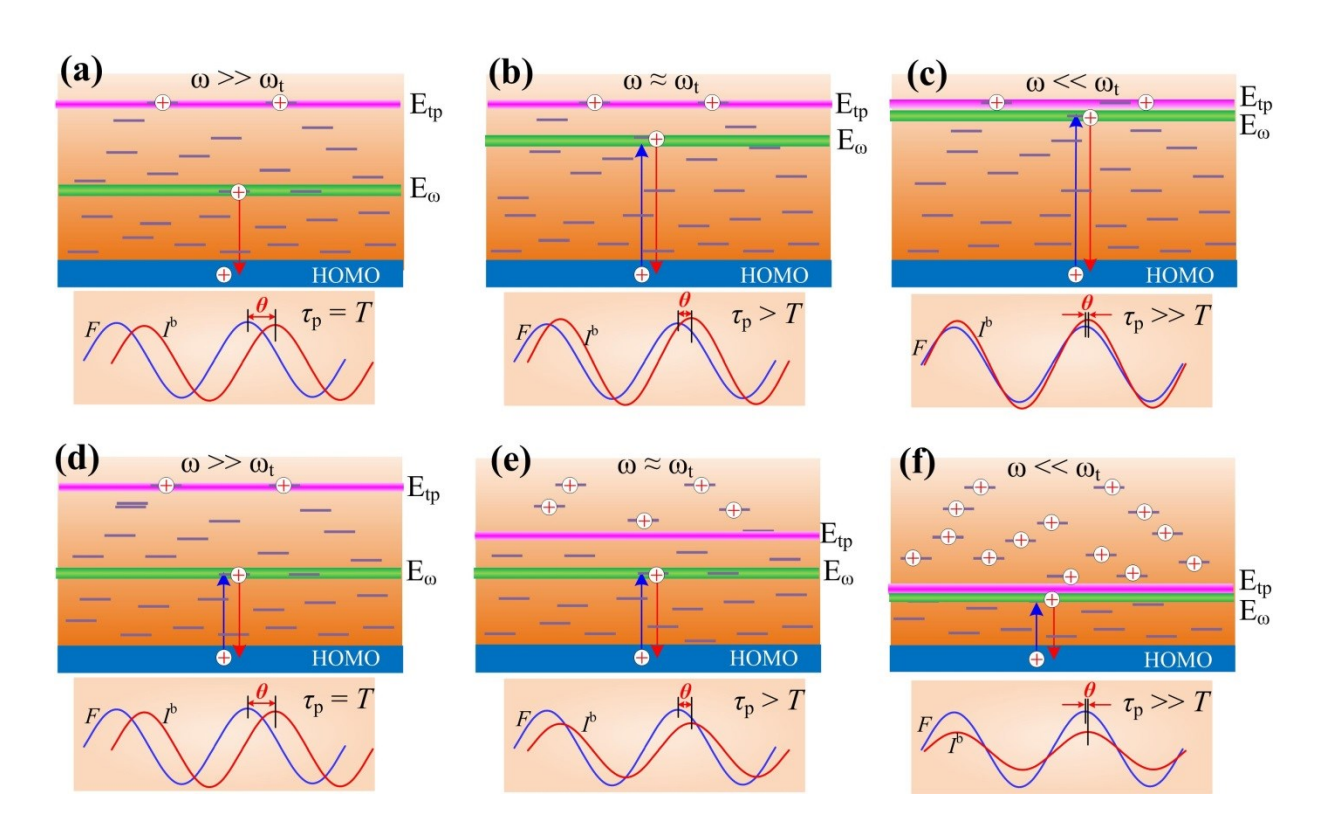


Figure 5. Illustration of relevant energy levels in MPC spectroscopy. The positions of the probed localized energy level E_{ω} (the horizontal green line) and the characteristic upmost filled trap level E_{tp} (the horizontal magenta line) are shown within the band gap of rubrene (orange background) together with other localized (trap) states (short black horizontal lines) and the HOMO edge (the dark blue band). Holes filling the traps up to E_{tp} level are also shown (white circles with "+" sign). The MPC phase shift θ and amplitude I^b are schematically shown at the bottom of each panel in comparison with the probe beam modulated at a frequency ω . The panels (a - c) correspond to a gradual transition from the HF ($\omega \gg \omega_t$) regime in panel (a) to the LF ($\omega \ll \omega_t$) regime in panel (c), occurring with increasing E_{ω} energy of the probed level (that is, via increasing its depth below the HOMO edge) due to a decreasing frequency of the probe beam ω . In this transition, ω first becomes closer to $\omega_{\rm t}$ ($\omega \approx$ ω_t), E_{ω} shifts closer to E_{tp} , the phase θ decreases, and I^b increases (panel b). At the lowest frequency $\omega \ll \omega_t$, θ becomes negligible, and I^b is high (panel c). Alternatively, the transition from the HF to the LF regime can occur when the intensity of the cw bias illumination increases, as shown in panels (d - f). In this case, ω_t becomes closer to ω , E_{tp} level moves closer to E_{ω} , populating more and more shallow states, the MPC phase θ and amplitude I^b both decrease (panel e). Eventually, at the highest bias light intensity, the LF regime is reached, when $\omega \ll \omega_t$, E_{tp} matches E_{ω} , θ is nearly zero, and I^b becomes nearly constant (panel f).

The rate, e_p , of thermal emission of carriers (holes) from the energy level E_{ω} at temperature T is:

$$e_{\rm p}(E_{\rm \omega}) = \frac{2\pi}{\tau_{\rm p}} = \nu_{\rm o} \exp(-E_{\rm \omega}/kT),\tag{1}$$

where τ_p is the thermal emission time from level E_{ω} (or, the carrier retention time), and v_0 is the attempt-to-escape frequency. The rate $e_p(E_{\omega})$ can be more generally defined as:

$$e_{\rm p}(E_{\omega}) = \sqrt{\omega^2 + \omega_t^2},\tag{2}$$

where ω is the modulation frequency of the probe beam, and ω_t is the characteristic trapping frequency given by $\omega_t = pc_p + nc_n$, with p and n representing the steady-state concentrations

of mobile holes and electrons (in cm⁻³) set by the intensity of the cw bias illumination, and c_p and c_n representing the coefficients of carrier capture (in cm³s⁻¹) on this specific trap state for holes and electrons, respectively. Considering for the sake of clarity only holes, we have $\omega_t \approx pc_p$, reflecting the fact that ω_t is controlled by the intensity of bias illumination. From Eqs. (1-2), the probed energy E_{ω} is thus given by:

$$E_{\omega} = kT \ln(\frac{v_0}{\sqrt{\omega^2 + \omega_t^2}}),\tag{3}$$

while the quasi-Fermi level corresponding to the upmost filled trap state E_{tp} is:

$$E_{\rm tp} = kT ln \left(\frac{\nu_{\rm o}}{\omega_{\rm t}}\right). \tag{4}$$

Therefore, for a given intensity of the bias beam and a given frequency ω of the probe beam, the trap state at E_{ω} defined by Eq. (3) would provide the maximum contribution to the MPC via trapping/detrapping processes. At a high probe's modulation frequency ($\omega >> \omega_t$), ω_t in Eqs. (2 - 3) can be neglected, and the thermal emission rate from the probed state at E_{ω} becomes equal to the modulation frequency of the probe beam, $e_p(E_{\omega}) \cong \omega$. Under these conditions, for E_{ω} and E_{tp} we get:

$$E_{\omega} \approx kT ln\left(\frac{v_{\rm o}}{\omega}\right), \quad E_{\rm tp} = kT ln\left(\frac{v_{\rm o}}{\omega_{\rm t}}\right), \quad and \quad E_{\omega} \ll E_{\rm tp}.$$
 (5)

Expressions (5) show that at $\omega >> \omega_t$ the probed energy level E_ω corresponds to shallow trap states, located much closer to the band edge than E_{tp} , as schematically illustrated in Fig. 5 (a) and (d). Correspondingly, all three values - the probed energy level E_ω , the MPC phase shift θ and amplitude I_{ac} - are nearly independent of ω_t and thus insensitive to the bias beam intensity. This situation corresponds to the high-frequency (HF) regime in the MPC spectra shown in Fig. 4.

When the modulation frequency ω decreases, the MPC spectra exhibit a transition from HF to LF regime, during which the probed energy level E_{ω} shifts closer to the quasi-Fermi level E_{tp} , as illustrated in Fig. 5 (b) and (c). Such a transition can be alternatively realized by

increasing the intensity of cw bias illumination, thus filling more traps and shifting the E_{tp} level closer to E_{ω} , as shown in Fig. 5 (e) and (f). In this regime, the characteristic frequency ω_t in Eqs. (2 - 3) is no longer negligible, indicating that the trapped holes are thermally emitted from the probed energy level E_{ω} within a time shorter than the probe beam's modulation period. Thus, holes trapped at E_{ω} have a comparatively shorter residence time, resulting in a smaller delay of the MPC signal, which accounts for the phase shift θ getting smaller and smaller with decreasing ω (Fig. 4 (a) and (c)).

Finally, the so-called low-frequency (LF) regime ($\omega \ll \omega_t$) is realized when either a very low probe's modulation frequency ω is used (Fig. 5(c)) or a high bias illumination intensity is applied (Fig. 5(f)). In this regime, Eqs. (2 - 4) yield $e(E_{\omega}) \cong \omega_t$, and E_{ω} and E_{tp} energies become comparable:

$$E_{\omega} \approx E_{\rm tp} = kT ln \left(\frac{v_{\rm o}}{\omega_{\rm t}}\right).$$
 (6)

Since in this regime the residence time of holes on the probed trap level is negligible compared to the probe beam's modulation period, the delay in MPC signal is negligible, which accounts for the nearly zero phase shift θ at low ω (Fig. 4 (a) and (b)). Moreover, in this LF regime, the MPC amplitude I_{ac} becomes almost independent of ω (plateau in Fig. 4 (b) and (d)), because E_{ω} is only weakly dependent on ω and barely shifts with varying ω , thus remaining in close proximity to E_{tp} level, which keeps I_{ac} signal nearly constant.

2. The density of free holes, hole mobility, and quasi-Fermi energy.

The shape of MPC spectra shown in Fig. 4 allows introducing the so-called onset frequency, ω_s , defined as the modulation frequency, at which a crossover from the HF to the LF regimes starts to occur. This crossover can be seen in $\theta(\omega)$ of pristine rubrene, when the phase starts to decrease with decreasing ω , before it reaches a nearly zero value (Fig. 4 (a)).

Alternatively, the crossover can also be identified in $I_{ab}(\omega)$, when the amplitude starts leveling off with decreasing ω , before it reaches a plateau (Fig. 4 (b)). It is clear from the data in Fig. 4 that the onset of this crossover significantly shifts to higher frequencies for higher intensities of bias illumination. This occurs due to an increase in the characteristic frequency ω_t , leading to a shift of the quasi-Fermi level E_{tp} to shallower energy levels. Thus, the onset frequency ω_s mirrors the movement of the quasi-Fermi level in the gap, which is, in turn, governed by the density of photogenerated carriers. This observation is consistent with the predictions of the MTR model.

It's worth noting that in the hopping transport regime applicable to disordered organic semiconductors, most of the carriers move via *hopping* between localized states. The effect of hopping on MPC spectra was modelled by Longeaud and Tobbeche [18]. It was found that photogenerated excess carriers undergoing hopping transport "condense" in the localized levels around the (dark) Fermi level position. As a consequence, the quasi-Fermi levels are found closer to the position of the dark Fermi level, compared to the case when only MTR is considered, and accordingly the free carrier density decreases. Thus, in a hopping-dominated transport regime, MPC should be almost insensitive to the bias illumination intensity, which would signify the prevalence of hopping transport [18]. This scenario clearly contradicts our experimental observations of the MPC spectral behavior in rubrene single crystals, both in pristine and in trap-dominated states of the crystal, thus ruling out hopping as the dominant transport mechanism. This is a reasonable conclusion since the present high quality rubrene crystals demonstrate a remarkable high mobility of the order $\mu \sim 20~\text{cm}^2\text{V}^{-1}\text{s}^{-1}$, which favors band transport according to MTR model. For this reason, the present crystals offered an experimental test bed of the unique ability of the modulated photocurrent experiment to signify predominance of band transport against hopping transport between the localized states. Note that steady state dark current or steady state photocurrent measurements fail to

detect contribution from hopping transport even in case where this mechanism predominates [18].

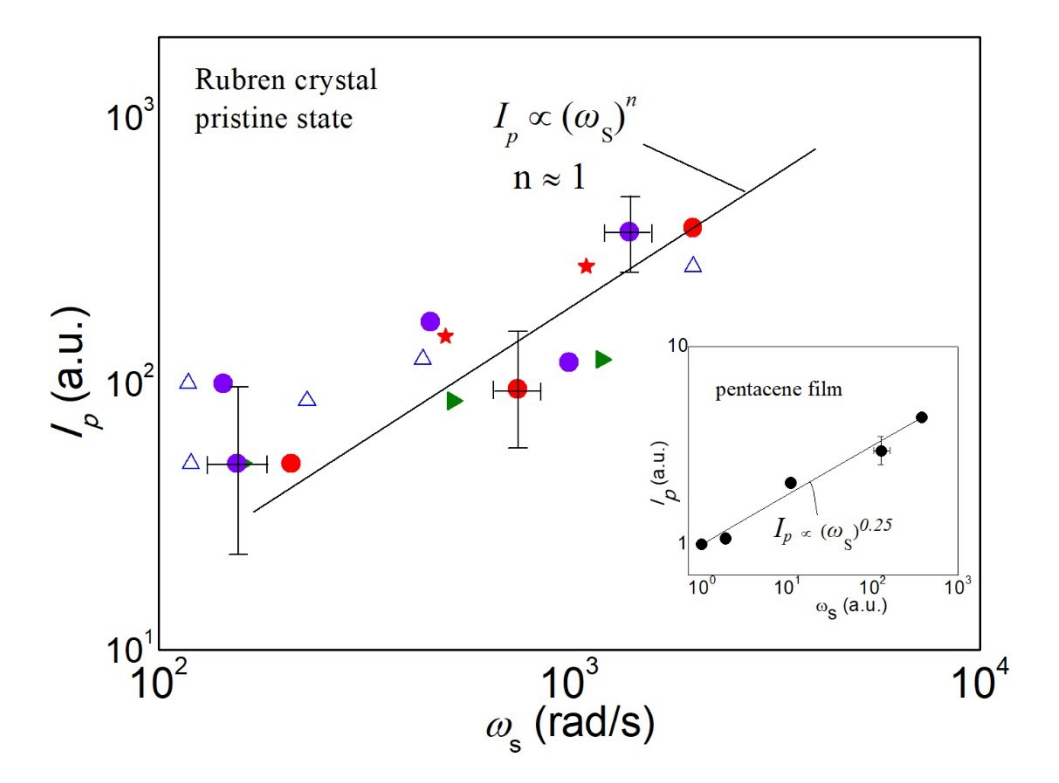


Figure 6. dc Photocurrent vs MPC onset frequency, $I_p(\omega_s)$, in pristine rubrene crystals. The data points correspond to measurements of a pristine rubrene single crystal under different intensities of bias illumination carrier ranging between about 1 and 10^4 nW/cm². It can be seen that an increase of the frequency ω_s by about one order of magnitude roughly corresponds to about one order of magnitude increase of the concurrently measured dc photocurrent I_p roughly following the solid line which is the linear relationship $I_p \propto (\omega_s)^n$ with n≈1. The approximate linearity of this relationship suggests that the mobility is carrier-density independent (Eq. (8)). Inset shows the respective $I_p(\omega_s)$ dependence of pentacene films which is a sublinear relationship with $I_p \propto (\omega_s)^n$ with n≈0.25. This is attributed to a decreasing mobility with increasing carrier-density due hole trapping into grain boundaries.

The onset frequency ω_s can be better determined from the MPC amplitude spectra due to the relatively smaller scatter in $I_{ac}(\omega)$ data (Fig. 4). Here, ω_s is the frequency, at which the MPC amplitude starts decreasing, when ω increases outside of the plateau region. Thus determined ω_s is found to increase approximately linearly with the concurrently measured dc photocurrent I_p . This is demonstrated in the plot of Fig. 6 which contains a large number of data points obtained in pristine rubrene at different levels of bias illumination. From this plot and despite the scattering of the experimental data, it is evident that an increase of the frequency ω_s by about one order of magnitude roughly corresponds to about one order of magnitude increase of the concurrently measured dc photocurrent I_p , indicating that I_p increases approximately linearly with the ω_s as: $I_p \propto (\omega_s)^n$, where $n \approx 1$ (solid line). The dc photocurrent I_p is proportional to the density-mobility product for mobile holes, $p\mu$:

$$I_{\rm p} = p\mu e E A,\tag{7}$$

where A is the effective cross-section area of the part of the crystal conducting the current, and $E \equiv V/L$ is the applied electric field, determined as the ratio of the applied voltage V to the conduction channel length L. When the bias illumination intensity increases, the density of holes p and the characteristic frequency $\omega_t = pc_p$ both increase. This can be monitored as an increasing onset frequency ω_s , because ω_t is expected to be proportional to ω_s [11]. Therefore, the hole density $p = \omega_t/c_p$ should be proportional to ω_s , and the photocurrent I_p should then be proportional to $\mu\omega_s$ product:

$$I_{\rm p} \propto \mu \omega_{\rm t} \propto \mu \omega_{\rm s}.$$
 (8)

The roughly linear relationship between I_p and ω_s observed for rubrene (Fig. 6) implies that the hole mobility μ in Eq. (8) remains essentially constant at different intensities of bias illumination. Namely, the mobility appears independent of the carrier concentration. This contradicts the carrier concentration dependence of the mobility predicted for hopping transport model in localized states with exponential energy distribution [19], like that of

rubrene [20-22] (see also next section). This makes unlike hopping transport, which was also concluded above from the strong light intensity dependence of the modulated photocurrent. Unlike the case of rubrene, similar measurements in polycrystalline pentacene films, which are included in the inset of Fig. 6 for comparison, reveal that an increase of the frequency of ω_s by three orders of magnitude, is related to a less than one order increase of the concurrently measured I_p . This shows that in pentacene films I_p increases with ω_s sub-linearly as: $I_p \propto (\omega_s)^n$, where $n \approx 0.25$, which is attributed to a decrease of hole mobility μ with increasing bias illumination intensity. Such a behavior in polycrystalline organic films can be explained by hole trapping at grain boundaries that increases the energy barriers for charge transport [11]. It is interesting that carrier trapping at grain boundaries and its effect on the Hall voltage has been recently revealed in Hall effect measurements of high-mobility polycrystalline thin-film OFETs [23]. Rubrene single crystals are free from grain boundaries, which is consistent with a constant μ observed here in $I_p(\omega_s)$ measurements.

A comparison of the onset frequencies and the respective photocurrents in pristine and trap-dominated states of rubrene allows examining the related degradation of carrier mobility caused by the gauge-effect treatment. The arrows and dotted lines in Fig. 4 (b) and (d) mark the two onset frequencies, ω_{s1} and ω_{s2} , corresponding to a relatively weak and a moderate bias illumination intensities, respectively, that generate the corresponding dc photocurrents, I_{p1} and I_{p2} . In the trap-dominated state (denoted below by primed variables), the bias beam intensity has been adjusted such that the onset frequencies ω_{s1} and ω_{s2} are roughly the same as those in the pristine state: $\omega_{s1} \approx \omega_{s1}$ and $\omega_{s2} \approx \omega_{s2}$. This is expected to lead to about the same concentrations of mobile holes in pristine and trap-dominated states of the crystal: $p_{s1} \approx p_{s1}$ and $p_{s2} \approx p_{s2}$, and thus to yield similar characteristic frequencies: $\omega_{t1} \approx p_{s1}c_p$ and $\omega_{t2} \approx p_{s2}c_p$. According to Eq. (8), similar dc photocurrents, I_{p1} and I_{p2} , should thus be observed in pristine and trap-dominated states of the sample under these illumination conditions.

However, our measurements show that the photocurrents I_{p1} and I_{p2} in the trap-dominated state are systematically lower than the corresponding photocurrents I_{p1} and I_{p2} in the pristine state by about a factor of 5 and 3, respectively. Following Eq. (8), the ratio of hole mobilities in the pristine and trap-dominated states of the crystal can be expressed as:

$$\frac{\mu}{\mu'} \approx \frac{I_{\rm p}}{I_{\rm p'}} \frac{\omega_{\rm s'}}{\omega_{\rm s}} \cong \frac{I_{\rm p}}{I_{\rm p'}} \approx 4. \tag{9}$$

Therefore our measurements show that the longitudinal photocarrier mobility at the surface of rubrene treated with a high-vacuum ion gauge is smaller than the pristine mobility by a factor of ~ 4 (on average), indicating that the high-vacuum gauge creates a significant additional electronic disorder (traps) at the surface of the crystals.

3. Estimating the DOS of localized states from the MPC spectra.

As shown above, MPC data in the HF regime (Fig. 4) are connected to the density $N(E_{\omega})$ of available in-gap states at the probed energy level E_{ω} given by Eq. (5). $N(E_{\omega})$ density can be obtained as [10]:

$$N(E_{\omega}) = \frac{2}{\pi} \frac{\mu e A}{c_{\rm p} k T} G E \frac{\sin \theta}{I_{\rm ac}}, \qquad (10)$$

where $G = (\eta \alpha F)/(hv)$ is a photogeneration rate, with F representing the r.m.s. of modulated incident illumination intensity (in W·cm⁻²), α is the optical absorption coefficient, hv is the photon energy of the probe beam, and η is the quantum efficiency of photocarrier generation. Assuming a band mobility of $\mu \sim 20 \text{ cm}^2\text{V}^{-1}\text{s}^{-1}$, a quantum efficiency $\eta = 0.001$ [15], an optical absorption coefficient $\alpha = 3500 \text{ cm}^{-1}$, and an attempt to escape frequency similar to that in pentacene, $v_0 \sim 10^{10} \text{ s}^{-1}$ (which is due to the capture coefficient of the order of $c_p \sim 10^{-11} \text{ cm}^3 \cdot \text{s}^{-1}$), we can estimate an order of magnitude of the DOS of in-gap localized states in the crystal.

Figure 7 shows this DOS for the pristine and trap-dominated states of the same rubrene crystal. A broad, nearly exponential DOS distribution in the form $N_{\rm v} \exp(-E/E_0)$, with a characteristic slope $E_0 \sim 33$ meV, is observed at very deep energies of 0.35 - 0.5 eV both in the pristine and in the trap-dominated states of the crystal. The DOS of the trap-dominated sample is however 1 - 2 orders of magnitude higher. At slightly lower energies of 0.3 - 0.35 eV, the DOS in the pristine state becomes steeper, with the characteristic slope of $E_0 \sim 21$ meV, which corresponds to the abrupt increase of the MPC phase θ seen in Fig. 4 (a) at higher ω .

Assuming attempt to escape frequency of the order $v_0 \sim 10^{10} \text{ s}^{-1}$, the calculated DOS is comparable to that obtained earlier in field-effect transistor (FET) and space-charge limited current (SCLC) measurements of rubrene [20-22]. Specifically, Blulle *et al* [20,21] found a

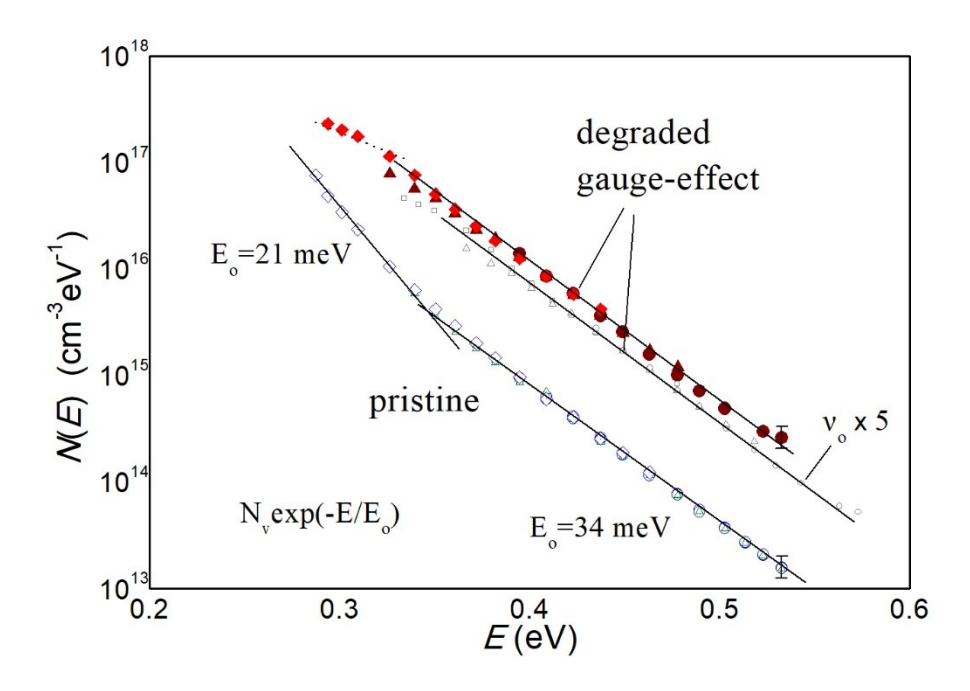


Figure 7. The density of localized (trap) states, N(E), in pristine and trap-dominated rubrene crystal. N(E) is calculated via Eq. (10). The trap-dominated ("degraded") state of

the crystal was prepared by briefly exposing the crystal to an operating high-vacuum ion gauge.

low deep trap density of the order of 1×10^{13} cm⁻³·eV⁻¹ around 0.6 eV below the transport level, which is similar to the deepest DOS of pristine rubrene in Fig. 7. Moreover, Blülle [21] reported an exponentially varying deep trap distribution, with almost the same characteristic slope as that in our deep DOS in Fig. 7, indicating that the MPC technique more likely probes the interaction of holes with the trap distribution in the tail of the HOMO band.

The DOS of the trap-dominated crystal is also calculated via Eq. (10), in which we took into account that the carrier mobility in this degraded state is reduced by a factor of ~ 4 (Fig. 7). A strong, 1 - 2 orders of magnitude increase in N(E) is observed at deep energies which stems from the strong decrease of the modulated photocurrent amplitude i_{ac} by about two orders of magnitude. The DOS distribution becomes slightly broader compared to the pristine state, with $E_0 \sim 35$ meV. In addition, the increase in the steepness of the DOS observed at shallower energies in the pristine state cannot be seen any more in the trapdominated state, which correlates well with the absence of a sharp upturn in θ at high ω in the degraded crystal (compare panels (a) and (c) of Fig. 4). It is worth noting that the defective surface of the crystal exposed to the ion gauge operation may also become more disordered facilitating capture of the mobile carrier by the traps increasing their capture coefficient, c_p and the attempt to escape frequency v_o by the same factor. A possible increase of c_p according to Eq. (10) is expected to decrease the calculated DOS, whereas the respective increase of v_o according to Eq. (6) shifts the energy range of E_{ω} at deeper trap depths. An example of the effect of a possible fivefold increase of c_p and v_o , in the calculated DOS of the degraded state is presented in Fig. 7 (small grey symbols). It can be seen that the thus calculated DOS distribution presents a small parallel shift to slightly lower DOS values and deeper energies.

Therefore, a possible increase of c_p and v_o by the gauge effect leaves the overall increase of the DOS essentially the same with that obtained assuming a constant c_p and v_o .

As mentioned above, assuming constant photogeneration rate G the strong decrease of the i_{ac} by the gauge effect according to Eq. (10) produces a strong increase of the calculated trap DOS (Fig. 7). However, the triplet excitons may encounter the extra created traps at the crystal's surface and may dissociate into mobile charge carriers resulting in higher quantum efficiency η producing higher photogeneration rate G in Eq. (10). If all the traps effectively contribute to exciton dissociation, then the increase of the trap N(E) density by the gauge effect should increases G by the same factor, so that according to Eq. (10) the modulated photocurrent amplitude, i_{ac} , should remain essential unchanged. In our case, a strong net decrease of i_{ac} is observed which through Eq. (10) estimates a strong increase of the trap DOS, without to consider any concomitant increase of G. If additionally there is increase of G from exciton dissociation by extra created traps, then introducing this increase of G in Eq. (10) an even higher N(E) is calculated by the same factor of increase of G, due to the extra trap density contributing to the enhanced dissociation of the excitons. Unfortunately, a possible increase of the G cannot be obtained from the present modulated photocurrent experiment. For this reason, our experiment estimates the net increase of the DOS of the traps which do not effectively contribute to exciton dissociation. Therefore the increase of the DOS of Fig. 7 is considered as a lower limit of the increase of the trap density by the gauge effect.

The drastic increase in the DOS of localized states of the crystal treated with an ion gauge also correlates well with the strong decrease of photoconductivity observed upon exposure of the sample to the gauge (Fig. 3), suggesting that additional traps created by the gauge may act as deep carrier recombination centers. Since such a high concentration of additional traps is induced here by a high-vacuum gauge, which has been previously shown to exert a short-range effect at surfaces, primarily affecting a nanoscale surface region of the crystal [12,14],

DOS in this surface layer of the crystal. This makes sense, given the unique photocarrier generation mechanism in rubrene that relies on the photoexcitation of triplet excitons in the bulk (via singlet fission), triplet exciton diffusion to the surface, and surface dissociation of triplets occurring almost exclusively at the surface of the crystal, irrespective of the light penetration length [14,15]. Thus, the trends observed here with the MPC spectroscopy are in line with the above mechanism of photoconductivity in rubrene.

4. The "gauge effect" on surface traps revealed via FET and Hall effect measurements.

In order to verify that extra electronic disorder (charge traps) has been generated at the surface of initially pristine rubrene single crystals by the so-called "gauge effect", we

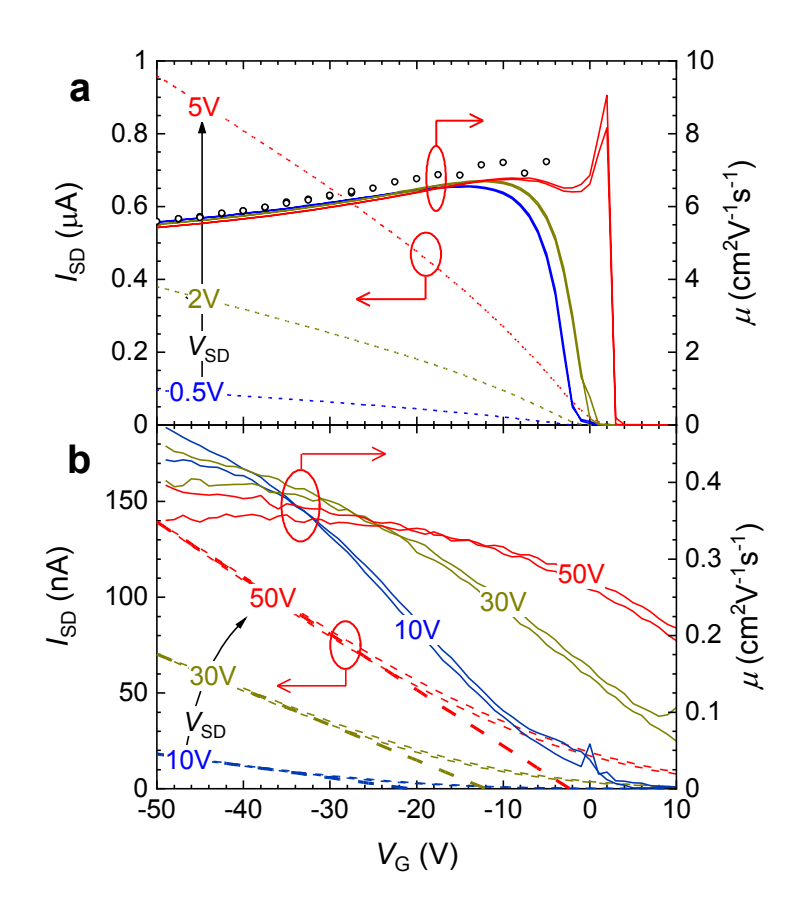


Figure 8. The "gauge effect" on the transport properties of single-crystal rubrene OFETs. (a)

A FET using a pristine rubrene single crystal, with the basic structure consisting of a macroscopic

The transfer characteristics $I_{\rm SD}(V_{\rm G})$ (dotted lines) and the field-effect mobility $\mu(V_{\rm G})$ (solid lines) measured at $V_{\rm SD}=0.5$, 2 and 5 V reveal a high-performance pristine FET. The mobility determined via Hall effect measurements is also shown (open circles). A match between the FET and Hall mobilities suggests a negligible density of traps at the crystal/dielectric interface. (b) A FET of analogous structure based on a crystal subjected to a gauge effect treatment right before the encapsulation in parylene-N gate dielectric. In this case, $I_{\rm SD}(V_{\rm G})$ and $\mu(V_{\rm G})$ characteristics recorded at $V_{\rm SD}=10$, 30 and 50 V suggest much greater densities of deep and shallow traps at the crystal's surface. The gate-channel capacitances per unit area of these devices are very similar: $C_{\rm i}=1.3-1.4$ nF-cm⁻². For the gauge-effect treatment conditions and FET fabrication see Methods section. These data clearly show that exposure of organic crystals to an operating high-vacuum gauge leads to a sharp increase in the trap concentration at their surface.

have made and characterized field-effect transistors prepared on pristine and "gauged" rubrene crystals. Exposing pristine bare rubrene crystals to an operating high-vacuum gauge in a high vacuum chamber leads to a rapid deactivation of its surface.

FET measurements of the device based on a pristine rubrene crystal and a similar device using a "gauged" crystal (both having comparable contact geometry and the parylene-N gate insulator of comparable thickness) are shown in Fig. 8. The transfer characteristics (the source-drain current I_{SD} vs. the gate voltage V_G) of the FETs based on pristine and gauged crystals are thus shown. The longitudinal FET mobility μ is calculated using the Shockley FET model for the linear regime and plotted as well [24]. The pristine device exhibits characteristics typical of a high-performance rubrene single-crystal OFET [25]. It is clear from these data that "gauging" drastically reduces the device's performance. Indeed, the carrier mobility has dropped by more than an order of magnitude (from $\mu \sim 6$ to ~ 0.4 cm²V⁻¹s⁻¹), which is stronger than the factor of 4 drop of μ deduced from the modulated photocurrent measurements. This is reasonable since the FET measurements sense the surface

of the crystal which is damaged by the gauge and where the accumulation channel of the OFET is formed. In contrast, the modulated photocurrent estimates a relatively lower drop of the mobility, because it gives an estimation of the average mobility from the surface layer which is damaged by the gauge and certain good part of the crystal below the surface within the penetration depth of the modulated light which is not damaged. The threshold voltage of the OFET has increased from nearly zero to more than 20 V (please note that a positive $V_{\rm SD}$ is applied in these p-type OFETs to the Source contact with respect to the grounded Drain, as listed in Fig. 5, which makes the onset point of the transfer characteristics to shift to positive $V_{\rm G}$ accordingly). This control experiment with FETs clearly shows that the surface of the crystal exposed to a gauge is trap dominated and thus expected to trap a lot more holes or even excitons than the surface of pristine crystals.

IV. CONCLUSIONS

We have studied high-performance organic semiconductors by a modulated photocurrent spectroscopy technique that takes advantage of the phase-sensitive detection of photoconductivity induced by a modulated excitation beam, with an additional control by a cw background illumination used to tune the mobile carrier density and adjust the position of quasi-Fermi level within localized states. In crystalline rubrene, this methodology allowed us to probe the charge transport mechanism, confirming its band-like nature, and scrutinize the effects of bias illumination and the high-vacuum ion gauge on the charge carrier mobility and the density of trap states. The MPC method reveals low but exponential distribution of deeptrap states that becomes steeper at shallower energies. After exposure of the crystals to an operating ion gauge, a strong decrease in the photocurrent response spectra is observed, which is especially prominent at the wavelengths of the strongest absorption. This behavior indicates that it is the surface layer of the crystal that is predominately affected by the ion

gauge via the generation of a substantial additional electronic disorder (traps) at the semiconductor's surface. Such a disorder would limit the surface charge transport, which agrees well with the observed mobility decrease by a factor of ~ 4, compared to the mobility of pristine crystals. Moreover, in the crystals degraded by the gauge effect, MPC measurements reveal a strong increase of the trap density (by about one-two orders of magnitude). The additional defects may act as photocarrier trapping cites and/or recombination centers, leading to the observed strong degradation of photoconductivity of the crystals exposed to the ion gauge.

Acknowledgement

V.P. acknowledges financial support from the National Science Foundation under Grant No.

ECCS-1806363

References:

- [1] Michael A. Fusella, Siyu Yang, Kevin Abbasi, Hyun Ho Choi, Zhuozhi Yao, Vitaly Podzorov, Amir Avishai, and Barry P. Rand *Chem. Mater.* 29, 6666 (2017).
- [2] R. A. Nawrocki, N. Matsuhisa, T. Yokota, T. Someya *Adv. Electron. Mater.* 2, 1500452 (2016).
- [3] A. Yamamura, S. Watanabe, M. Uno, M. Mitani, C. Mitsui, J. Tsurumi, N. Isahaya, Y. Kanaoka, T. Okamoto, J. Takeya, *Sci. Adv.* 4, 5758 (2018).
- [4] M. A. Fusella, A. N., M. Welborn, G. E. Purdum, Y. Yan, R. D. Schaller, Y. H. L. Lin, Y. L. Loo, T. V. Voorhis, N. C. Giebink, B. P. Rand Adv. Energy Mater. 8, 1701494 (2018).
- [5] P. Irkhin, I. Biaggio, T. Zimmerling, M. Döbeli, and B. Batlogg, *Appl. Phys. Lett.* 108, 063302 (2016).
- [6] L. Basiricò, A. Ciavatti, T. Cramer, P. Cosseddu, A. Bonfiglio, B. Fraboni, *Nat. Commun.* 7, 13063 (2016).
- [7] L. Carman, H. P. Martinez, L. V. Steven Hunter, P. Beck, N. Zaitseva, S. A. Payne, P. Irkhin, H. H. Choi, V. Podzorov, *IEEE Trans Nucl Sci.* 64, 781 (2017).
- [8] J. Day, S. Subramanian, J. E. Anthony, Z. Lu, R. J. Twieg, O. Ostroverkhova, *J. Appl. Phys.* 103, 123715 (2008).
- [9] F. Ortmann, F. Bechstedt, K. Hannewald, *Phys Status Solidi B* 248, 511 (2011).
- [10]. M. Pomoni, A. Giannopoulou and P. Kounavis, *Philos. Mag.* 90, 3441 (2010).
- [11]. N. Vagenas, A. Giannopoulou, and P. Kounavis, J. App. Phys. 117, 033105 (2015).
- [12]. V. Podzorov, E. Menard, S. Pereversev, B. Yakshinsky, T. Madey, J. A. Rogers, M. E. Gershenson, *Appl. Phys. Lett.* 87, 093505 (2005).

- [13]. R. W. I. de Boer, M. E. Gershenson, A. F. Morpurgo, V. Podzorov, *Phys. Stat. Sol.* (a) 201 1302 (2004).
- [14]. P. Irkhin, H. Najafov, V. Podzorov, Sci Rep Sci Rep. 5, 15323 (2015).
- [15]. H. Najafov, B. Lee, Q. Zhou, L. C. Feldman, V. Podzorov, *Nature Mater.* 9, 938 (2010).
- [16]. V. Podzorov, MRS Bulletin 38, 15 (2013).
- [17] V. Podzorov, E. Menard, A. Borissov, V. Kiryukhin, J. A. Rogers, and M. E. Gershenson, *Phys. Rev. Lett.* 93, 086602 (2004).
- [18]. C Longeaud and S Tobbeche, J. Phys.: Condens. Matt, 21, 045508 (2009).
- [19]. S. D. Baranovskii, Phys. Status Solidi B 251, 487 (2014)
- [20] B. Blülle, R. Häusermann, B. Batlogg Phys. Rev. Applied 1, 034006 (2014).
- [21]. B. Blülle, 2016, Doctoral Thesis, ETH Sürich Permanent link

https://doi.org/10.3929/ethz-a-010718150.

- [22] J. Dacuña, A. Salleo, *Phys. Rev. B* 84, 195209 (2011).
- [23]. H. H. Choi, A. F. Paterson, M. A. Fusella, J. Panidi, O. Solomeshch, N. Tessler, M. Heeney, K. Cho, T. D. Anthopoulos, B. P. Rand, V. Podzorov, *Adv. Funct. Mater.* 30, 1903617 (2019).
- [24] H. H. Choi, K. Cho, C. D. Frisbie, H. Sirringhaus, V. Podzorov, Nat. Mater., 17, 2 (2018).
- [25] V. Podzorov, S. E. Sysoev, E. Loginova, V. M. Pudalov, M. E. Gershenson, Appl. Phys. Lett., 83, 3504 (2003).